Free Surface Tracking for the Accurate Time Response Analysis of Nonlinear Liquid Sloshing

Jin-Rae Cho*, **Hong-Woo Lee**
School of Mechanical Engineering, Pusan National University,
Busan 609-735, Korea

Liquid sloshing displays the highly nonlinear free surface fluctuation when either the external excitation is of large amplitude or its frequency approaches natural sloshing frequencies. Naturally, the accurate tracking of time-varying free surface configuration becomes a key task for the reliable prediction of the sloshing time-history response. However, the numerical instability and dissipation may occur in the nonlinear sloshing analysis, particularly in the long-time beating simulation, when two simulation parameters, the relative time-increment parameter α and the fluid mesh pattern, are not elaborately chosen. This paper intends to examine the effects of these two parameters on the potential-based nonlinear finite element method introduced for the large amplitude sloshing flow.

Key Words : Large Amplitude Sloshing, Nonlinear Finite Element Analysis, Numerical Instability and Dissipation, Relative Time-Increment Parameter, Fluid Mesh Pattern

1. Introduction

One of the major issues in the numerical analysis of large amplitude liquid sloshing is a free surface tracking. It is because the free surface configuration plays an important role not only in the flow domain identification but also as the kinematic and dynamic boundary conditions of initial-boundary-value sloshing problem. In addition, a small error in the free surface tracking, which is to be accumulated with the time integration stage, may cause the numerical dissipation and instability in the time response analysis of nonlinear liquid sloshing (Chen et al., 1996).

In order for the accurate time tacking of the free surface configuration, various useful techniques have been introduced. Nakayama and

---
* Corresponding Author,
  E-mail : jrcho@pusan.ac.kr
  TEL : +82-51-510-2467; **FAX** : +82-51-514-7640
  School of Mechanical Engineering, Pusan National University, Busan 609-735, Korea. (Manuscript **Received** January 12, 2005; **Revised** May 20, 2005)

Washizu (1981) introduced an error correction term into the dynamic boundary condition for the boundary element formulation, and Okamoto and Kawahara (1990) proposed the velocity correction method based on the Lagrangian FEM formulation. Chen et al.(1996) used the implicit finite difference method based on the Crank-Nicolson time marching scheme in which second-order numerical dissipation term was added to the kinematic boundary condition to suppress the numerical instability. On the other hand, Kanok-Nukulchai and Tam (1999) introduced a large-displacement fluid element based on total Lagrangian formulation by employing the penalty method to enforce the liquid incompressibility.

In the current study, the free surface configuration is tracked by time-integrating the kinematic and dynamic boundary conditions making use of a forward-difference time differentiation of the free surface elevation and the predictor-corrector method incorporated with the mass-conservative remeshing scheme (Cho and Lee, 2003). The problem itself is formulated based upon the fully nonlinear potential flow theory, so that the state

variable is the velocity potential. Meanwhile, according to the least square method, the flow velocity field is interpolated from the velocity potential field approximated, with second-order finite elements.

The kinematic boundary condition governing the free surface configuration includes a convection term (Currie, 1974), and which has been a critical cause leading to the difficulty in the free-surface time tracking. In order to avoid the difficulty in dealing with the convection term, we devise an alternative technique to time-integrate the kinematic boundary condition. We directly evaluate the time derivative of the free surface elevation according to the forward difference scheme and then update the free surface configuration making use of the predictor-corrector method (Gill and Cullen, 1992). The time increment δt for the forward difference scheme is controlled by a parameter $\alpha(0<\alpha\leq1)$ defined as the relative ratio to the time step size Δt. Then, the choice of α affects the numerical accuracy and stability in the free surface time tracking. Besides, the fluid mesh pattern does also influence the free surface tracking accuracy even though the total liquid volume is kept unchanged by the above-mentioned remeshing scheme. It is because the large amplitude liquid sloshing shows a high singularity in the flow field near the free surface.

The purpose of the current study is to examine the reliability of the free surface tracking technique introduced into the potential-based nonlinear finite element method for large amplitude sloshing flow. In particular, the main observation focuses on the effects of two key parameters, the relative time-increment parameter α and the fluid mesh pattern, on the numerical stability and dissipation.

2. Problem Description

We consider a sloshing flow of inviscid incompressible liquid in a two-dimensional rigid tank of width $2d$ subjected to a forced horizontal excitation. In the stationary condition, liquid is filled up to the height H_L. For mathematical description purpose, we use two Cartesian co-
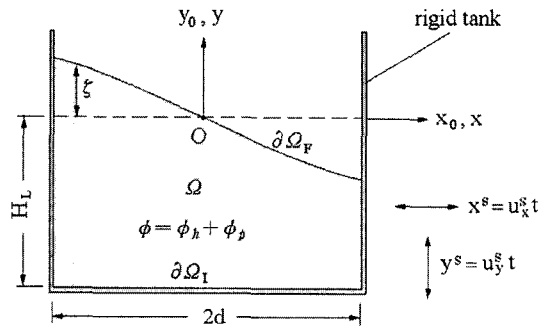

Fig. 1 Liquid contained in 2-D rigid tank subject to forced excitation

ordinate systems, $\{X_0\}$ fixed in space and $\{X\}$ moving with the tank, such that their origins are at the center of the stationary free surface and their axes are taken parallel to each other. Then, a scalar quantity Φ can be expressed in either of two co-ordinate systems such that $\Phi(x_0, y_0; t) = \widetilde{\Phi}(x, y; t)$. By denoting $\boldsymbol{u}^s(t) = \{dx^s/dt, dy^s/dt\}$ be the rigid tank velocity, we have the relations between two systems:

$$\frac{\partial\Phi}{\partial t}\bigg|_{\{X_0\}}=\frac{\partial\widetilde{\Phi}}{\partial t}\bigg|_{\{X\}}-\boldsymbol{u}^s\cdot\nabla\widetilde{\Phi} \qquad (1)$$

$$\nabla\Phi|_{\{X_0\}}=\nabla\widetilde{\Phi}|_{\{X\}} \qquad (2)$$

Hereafter, the subscript 0 refers to the quantities measured in the fixed Cartesian co-ordinates.

By denoting $\phi(x_0, y_0; t)$ be the velocity potential, the continuity condition is described by the Laplace equation:

$$\nabla^2\phi=0, \text{ in } \Omega^t \qquad (3)$$

On the liquid-structure interface, the velocity potential should satisfy

$$\nabla\phi\cdot\boldsymbol{n}=\boldsymbol{u}^s\cdot\boldsymbol{n}, \text{ on } \partial\Omega_I^t \qquad (4)$$

with the outward unit vector $\boldsymbol{n}$ normal to the structure boundary. In the fixed Cartesian co-ordinates, the kinematic and dynamic conditions on the free surface are as follows:

$$\frac{\partial\eta_0}{\partial t}+\frac{\partial\phi}{\partial x_0}\frac{\partial\zeta_0}{\partial x_0}-\frac{\partial\phi}{\partial y_0}=0, \text{ on } \partial\Omega_F^t \qquad (5)$$

$$\frac{\partial\phi}{\partial t}+\frac{1}{2}\nabla\phi\cdot\nabla\phi+g\zeta_0=0, \text{ on } \partial\Omega_F^t \qquad (6)$$

in which $\zeta_0(x_0 ; t)$ is the vertical coordinate $y_0(x_0 ; t)$ of the free surface.

Since the free surface fluctuation is a relative motion with respect to the container, the moving coordinates is usually preferable. By denoting $\zeta(x ; t) = \zeta_0(x_0 ; t) - y^s(t)$ be the free surface elevation from the reference stationary level, together with Eqs. (1) and (2), above free surface conditions are rewritten as

$$\frac{\partial \zeta}{\partial t} + \left(\frac{\partial \phi}{\partial x} - u_x^s\right)\frac{\partial \zeta}{\partial x} - \left(\frac{\partial \phi}{\partial y} - u_y^s\right) = 0 \quad (7)$$

$$\frac{\partial \phi}{\partial t} - \boldsymbol{u}^s \cdot \nabla \phi + \frac{1}{2}\nabla \phi \cdot \nabla \phi + g\,(\zeta + y^s) = 0 \quad (8)$$

In the moving co-ordinate system, the velocity potential $\phi(x, y ; t)$ can be split into two parts, $\phi_h(x, y ; t)$ due to the internal sloshing flow and $\phi_p(x, y ; t)$ due to the tank motion, such that

$$\phi = \phi_h + \phi_p, \quad \phi_p = x u_x^s + y u_y^s \quad (9)$$

Substituting Eq. (9) into Eqs. (7) and (8) we have

$$\frac{\partial \zeta}{\partial t} + \frac{\partial \phi_h}{\partial x}\frac{\partial \zeta}{\partial x} - \frac{\partial \phi_h}{\partial y} = 0 \quad (10)$$

$$\frac{\partial \phi_h}{\partial t} + \frac{1}{2}\nabla \phi_h \cdot \nabla \phi_h + g\zeta + x\frac{du_x^s}{dt} + \zeta\frac{du_y^s}{dt}$$
$$= \frac{1}{2}|\boldsymbol{u}^s|^2 - gy^s \quad (11)$$

It is worth to note that the RHS in Eq. (11) can be deleted because not only both terms are coordinate-independent quantities but also the velocity potential is a relative quantity in space.

Then, the initial-boundary-value problem of nonlinear sloshing flow in the moving co-ordinate system is formulated as follows:

$$\nabla^2 \phi_h = 0, \text{ in } \Omega^t \quad (12)$$

with initial conditions

$$\phi_h = -x u_x^s(0) - y u_y^s(0), \text{ in } \Omega^0 \quad (13)$$

$$\zeta = 0, \text{ on } \partial \Omega_F^0 \quad (14)$$

and boundary conditions

$$\nabla \phi_h \cdot \boldsymbol{n} = 0, \text{ on } \partial \Omega_I^t \quad (15)$$

$$\frac{\partial \zeta}{\partial t} = -\frac{\partial \phi_h}{\partial x}\frac{\partial \zeta}{\partial x} + \frac{\partial \phi_h}{\partial y}, \text{ on } \partial \Omega_F^t \quad (16)$$

$$\frac{\partial \phi_h}{\partial t} = -\frac{1}{2}\nabla \phi_h \cdot \nabla \phi_h - g\zeta - x\frac{du_x^s}{dt}$$
$$- \zeta\frac{du_y^s}{dt}, \text{ on } \partial \Omega_F^t \quad (17)$$

3. Time-Incremental Finite Element Approximation

In order to solve the above nonlinear sloshing problem we divide the observation time interval t into a finite number of sub-intervals such that $t_n = n\Delta t\,(n = 0, 1, 2, \cdots)$. With initial conditions (13)-(14) and the boundary condition (15), we solve the Laplace equation (12) defined in initial flow domain Ω^0 and boundary $\partial \Omega^0$ to seek ϕ_h^0. With which we compute the flow velocity field v^0 and perform the free surface tracking. By time-integrating the kinematic and dynamic boundary conditions (16)-(17), we identify ζ^1, Ω^1 and $\partial \Omega^1$. In this manner, the sloshing time response is to be numerically analyzed.

Referring to Fig. 2, we consider time stage t_n at which ϕ_h^n and $\boldsymbol{v}^n$ are to be sought with the geometry and field quantities determined at time stage t_{n-1}. According to the Galerkin method, we have the weak form of Eq. (12): find ϕ_h^n such that

$$\int_{\Omega^n} \nabla \psi \cdot \nabla \phi_h^n dv = 0 \quad (18)$$

for every admissible velocity potential $\psi(x, y)$. The corresponding essential boundary condition on $\partial \Omega_F^n$ is ϕ_h^n determined beforehand by the free surface tracking method described later.

By introducing nine-node Lagrange-type finite element basis functions $\{N_i\}_{i=1}^N$ and the nodal potential vector $\bar{\phi}_h^n$, we approximate
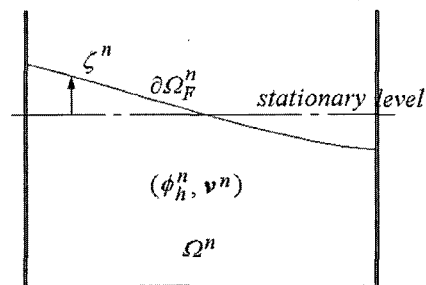

Fig. 2 Sloshing flow configuration at time stage t_n

$$\phi_h^n = N \circ \overline{\phi}_h^n \qquad (19)$$

Substituting Eq. (19) into Eq. (18) leads to

$$K \overline{\phi}_h^n = 0 \qquad (20)$$

with the matrix K defined by

$$K = \int_{\Omega^n} (\nabla N)^T (\nabla N) \, dv \qquad (21)$$

From the velocity potential ϕ_h^n approximated, the intermediate velocity field $\overline{v}^n$ is computed according to

$$\overline{v}^n = \nabla N \circ \overline{\phi}_h^n \qquad (22)$$

Owing to the C^0 continuity in the velocity potential field, the intermediate velocity field becomes to be discontinuous across element interfaces. One may consider the linear interpolation of the velocity values at Gauss integration points in order to obtain the continuous velocity field with the better accuracy. However, a small error in the velocity computation does not only affect the accuracy in the free surface tracking but also accumulate with the time stage. In order to minimize this crucial problem, we first interpolate element-wise velocity fields with second-order polynomials according to the least square method. Let us denote $\hat{v}_\alpha^n (\alpha = x, y)$ be the element-wise velocity components to be interpolated:

$$\hat{v}_\alpha^n = a_1 + a_2 \xi + a_3 \eta + a_4 \zeta \eta + a_5 \xi^2 + a_6 \eta^2 \qquad (23)$$

And we define the element-wise errors by

$$\Re_\alpha = \sum_{l=1}^9 \{ \hat{v}_\alpha^n(\xi_l, \eta_l) - \overline{v}_\alpha^n(\xi_l, \eta_l) \}^2, \ \alpha = x, y \qquad (24)$$

where l stand for (3×3) Gauss integration points. Then, six coefficients involved in each velocity component are determined from six simultaneous equations constructed from

$$\frac{\partial \Re_\alpha}{\partial a_k} = 0, \ k = 1, 2, \cdots, 6 \qquad (25)$$

From $\hat{v}_\alpha^n$ interpolated, we next calculate the velocity values for individual elements and average the nodal values for the common nodes. Finally, the global continuous velocity field is interpolated using the same finite element basis functions used in Eq. (19) and the component-wise

nodal velocity vectors $\overline{v}_\alpha^n$:

$$v_\alpha^n = N \circ \overline{v}_\alpha^n, \ \alpha = x, y \qquad (26)$$

4. Free Surface Tracking

After obtaining the velocity potential and the flow velocity field, we integrate Eq. (16) to track the free surface ζ^{n+1} and Eq. (17) to determine the essential boundary condition ϕ_h^{n+1}. A mass-conservative remeshing process follows the free surface tracking, while keeping the mesh regularity, in order to update the liquid mesh. In the kinematic boundary condition (16), the major feature is the convection term in the right-hand-side. The influence of this term increases as the sloshing amplitude becomes larger, and which may cause the numerical divergence, the high frequency wiggle or the numerical dissipation, in the sloshing time response (Chen et al., 1996), unless any special care is paid in the free surface tracking. In the present study, we introduce the direct differentiation to track the free surface without causing the numerical instability.

Referring to Fig. 3, we predict the free surface variation in the small time increment $\delta t (\delta t = \alpha \Delta t, 0 < \alpha \leq 1)$ from the current time t_n according to

$$x_i' = x_i + \delta t \left. \frac{\partial \phi_h}{\partial x} \right|_{(x_i, y_i)}$$
$$y_i' = y_i + \delta t \left. \frac{\partial \phi_h}{\partial y} \right|_{(x_i, y_i)} \qquad (27)$$

Here, α is defined by the relative time increment parameter and (x_i, y_i) the coordinates of node
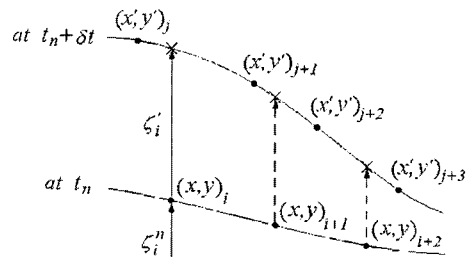

Fig. 3 Variation of the free surface in the time increment δt

i on the free surface at time t_n. And, the elevation of node i in the time increment δt can be calculated through

$$\zeta_i' = y_j^1 + \frac{y_{j+1}' - y_j'}{x_{j+1}' - x_j'}(x_i - x_j') \tag{28}$$

Then, the time derivative of the free surface elevation in Eq. (16) is directly calculated by the forward difference scheme

$$\left.\frac{\partial \zeta}{\partial t}\right|_n \approx \left.\frac{\delta \zeta}{\delta t}\right|_n = \frac{\zeta' - \zeta^n}{\delta t} \tag{29}$$

We next apply the predictor-corrector method composed of the explicit fourth-order Adams-Bashforth scheme (Golub and Ortega, 1992) and the implicit fourth-order Adams-Moulton scheme (Golub and Ortega, 1992) given respectively by

$$\tilde{\zeta}^{n+1} = \zeta^n + \frac{\Delta t}{24}\left[55\left.\frac{\partial \zeta}{\partial t}\right|_n - 59\left.\frac{\partial \zeta}{\partial t}\right|_{n-1} \right. $$
$$\left. + 37\left.\frac{\partial \zeta}{\partial t}\right|_{n-2} - 9\left.\frac{\partial \zeta}{\partial t}\right|_{n-3}\right] \tag{30}$$

$$\zeta^{n+1} = \zeta^n + \frac{\Delta t}{24}\left[9\left.\frac{\partial \tilde{\zeta}}{\partial t}\right|_{n+1} + 19\left.\frac{\partial \zeta}{\partial t}\right|_n \right. $$
$$\left. - 5\left.\frac{\partial \zeta}{\partial t}\right|_{n-1} + \left.\frac{\partial \zeta}{\partial t}\right|_{n-2}\right] \tag{31}$$

in order to predict the free surface elevation at the next time stage t_{n+1}. Then, we relocate the free surface nodes onto the new free surface $\partial \Omega_F^{n+1}$ by moving only in the vertical direction, as depicted in Fig. 4(a). As well, we calculate the total liquid area according to the trapezoidal rule

$$A_{tot} = \sum_{i=1}^{K} A_i, \quad A_i = (x_{i+1} - x_i)\frac{\zeta_{i+1} + \zeta_i}{2} \tag{32}$$

Then, the mean free-surface elevation ζ_{mean} can be calculated as follows : $\zeta_{mean} = A_{tot}/2d$ and the nodal free surface heights ζ_i^{n+1} are corrected (Cho and Lee, 2003) such that $\zeta_i^{n+1} = \zeta_i^{n+1} - \zeta_{mean}$.

We next relocate all of internal nodes such that finite element nodes located in the same vertical line are in uniform spacing. In this manner, the free surface is tracked by keeping the liquid mesh unchanged and the liquid mesh is adapted so as to keep the mesh regularity fairly. As a next step,
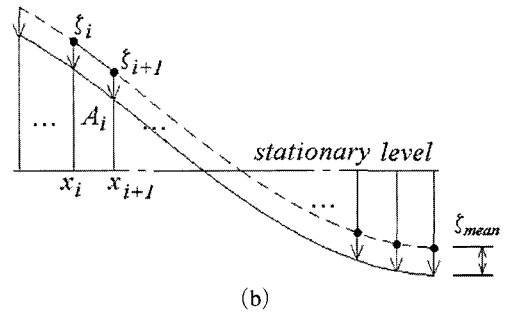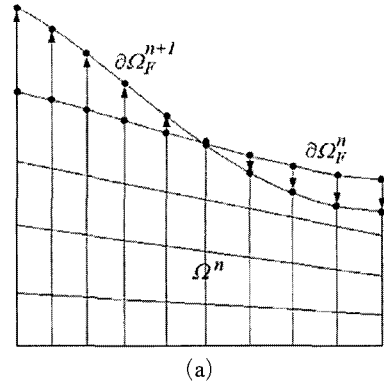

(a)

(b)

Fig. 4 Volume-conservative remeshing : (a) Relocation of finite element nodes ; and (b) Correction of the free surface nodes

we integrate Eq. (17) to specify the velocity potential ϕ_h^{n+1} at the free surface $\partial \Omega_F^{n+1}$ tracked. However, the time derivative of the free surface velocity potential in the moving co-ordinate system $\{X\}$ is related to one in the semi-Lagrangian liquid mesh $\{X_M\}$ as follows :

$$\left.\frac{\partial \phi_h}{\partial t}\right|_{\{X\}} = \left.\frac{\partial \phi_h}{\partial t}\right|_{\{X_M\}} - \frac{\partial \zeta}{\partial t}\frac{\partial \phi_h}{\partial y} \tag{34}$$

Thus, with respect to the liquid mesh, the time derivative of the free surface velocity potential at time stage t_n is rewritten as

$$\left.\frac{\partial \phi_h}{\partial t}\right|_n = \left.\frac{\partial \zeta}{\partial t}\right|_n \frac{\partial \phi_h^n}{\partial y} - \frac{1}{2}\nabla \phi_h^n \cdot \nabla \phi_h^n $$
$$- g\zeta^n - x\frac{du_x^s}{dt} - \zeta^n \frac{du_y^s}{dt}, \text{ on } \partial \Omega_F^n \tag{35}$$

After computing this time derivative, we apply the same predictor-corrector method as in the free surface tracking to specify the velocity potential ϕ_h^{n+1} on the new free surface $\partial \Omega_F^{n+1}$.

5. Numerical Experiments

The numerical formulae derived so far were coded into a test program written in Fortran, and MSC/Patran was interfaced for the output visualization. Referring to Fig. 1, we confine to large amplitude sloshing problems in which the rigid tank is subject to a sinusoidal horizontal excitation $x^s(t) = a \sin \omega t$. Based upon the literature survey on the nonlinear sloshing analysis we consider two simulation cases. Geometry and excitation conditions of case 1 which was taken by Chen et al.(1996) and Okamoto and Kawahara (1990) are as follows : $d = 1.0$ m, $H_L = 0.5$ m, $a = -9.3 \times 10^{-3}$ m and $\omega = 0.9995 \omega_0$ (here, the fundamental sloshing frequency ω_0 is 5.31384 rad/s). On the other hand, those of case 2 chosen by Nakayama and Washizu (1981) are d of 0.9 m, H_L of 0.6 m, a of 2×10^{-3} m and $\omega = 0.9547 \omega_0$ ($\omega_0 = 5.76077$ rad/s), respectively.

In the beginning, the liquid domains in both simulation cases were uniformly discretized with nine-node quadratic elements in the manner of 24 partitions in the horizontal direction and 12 partitions in the vertical direction. The time step size Δt was set by 5×10^{-3} s for all simulation cases presented in this paper. The predictor-corrector method composed of two fourth-order schemes (30) and (31) is known as a highly accurate time integration scheme with the truncation error of $(\Delta t)^4$. In addition, the time step size was chosen through the preliminary parametric convergence experiments to the tank width, the liquid depth and the excitation amplitude and frequency.

We first examine the effect of the parameter α on the numerical dissipation and the liquid volume change. This numerical experiment was done with case 1 because the sloshing nonlinearity is higher than case 2. It is worthy noting that this preliminary simulation was performed without correcting the free-surface height according to Eq. (33) so that errors in the free surface height and the total liquid volume are allowed to accumulate with time. Referring to Fig. 5(a), the numerical dissipation is getting suppressed as α
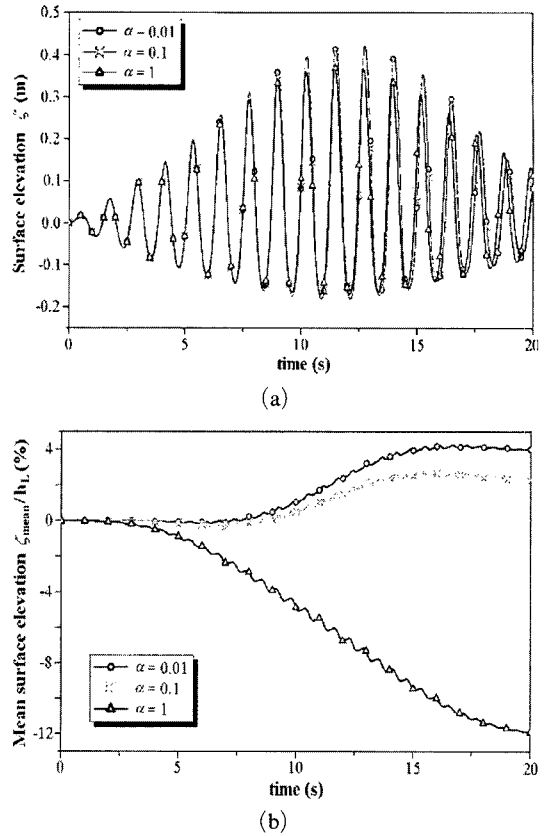

(a)

(b)

Fig. 5 Effects of the parameter α : (a) On the free surface elevation (at the right end $x = 0.5$ m) ; (b) On the liquid volume conservation

becomes smaller such that the time history responses of the free surface elevation at $\alpha = 0.1$ and 0.01 do not show a noticeable distinction. On the other hand, the total liquid volume, referring to Fig. 5(b), considerably decreases when α is unity, and contrary it slightly increases when $\alpha \leq 0.1$. From these results, we found that the choice of α near 0.1 is recommendable.

Next, we examine the effects of the fluid mesh pattern on the time history response of the free surface elevation with α set by 0.1. Uniform mesh and locally refined meshes are to be tested for the numerical stability and dissipation in two simulation cases. In case 1, we simulate the long-time response of the large beating phenomenon to examine the numerical dissipation with time. On the other hand, in case 2, we examine the numerical stability in the short-time history response by

comparing with the existing reference solution. Differing from the real liquid sloshing including the damping effect, its numerical simulation with an ideal flow assumption should keep the same amplitude in repeating events unless the numerical dissipation does accumulate (Faltinsen et al., 2000).

Long- and short-time history responses predicted by the uniform mesh of the free surface elevation in cases 1 and 2 are represented respectively in Figs. 6(a) and 6(b). Two uniform meshes for both simulation cases are generated with the same mesh partitions (i.e. 24 times 12) and the free surface elevations are measured at the right ends (i.e. at $x=0.5$ m in case 1 and $x=0.45$ m in case 2). Referring to Fig. 6(a), one see that the uniform mesh failed to simulate the beating phenomenon such that not only the first beating wave is getting to be distorted but also the beating amplitude shows a monotonic decrease with the increase of beating events. Furthermore, the

uniform mesh produces the numerical instability at the beginning of the free surface time history, as indicated by circle A in Fig. 6(b). Differing from the reference solution, the free surface response predicted by the uniform mesh starts with a downward fluctuation.

The main reason leading to these poor results is because the uniform mesh could not sufficiently capture the flow singularity. As shown in Fig. 7 (a), a large amplitude liquid sloshing exhibits the significant singularities in both flow velocity and dynamic pressure fields at the free surface and left and right ends of tank. Referring to the paper by Cho and Oden (1997), an effective way to capture the singularity is to use locally refined meshes. So, we refine the both uniform meshes in the manner represented in Fig. 7(b).

As represented in Fig. 8(a), the locally refined mesh successfully prevents the numerical dissipation occurred in the long-time history response of the large beating phenomenon such that beating events display almost same wave patterns and
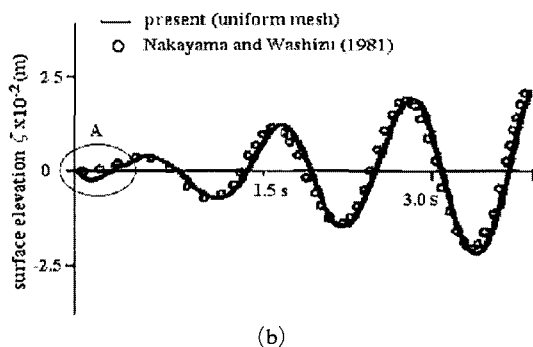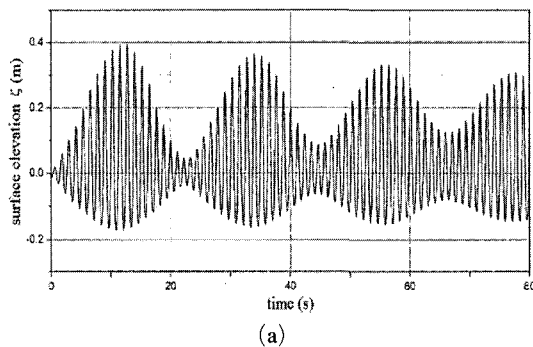

(a)

(b)

Fig. 6 Use of uniform mesh : (a) Long-time history of the beating phenomenon (case 1); (b) Numerical instability at the beginning (case 2)

$t = 12.77$ s
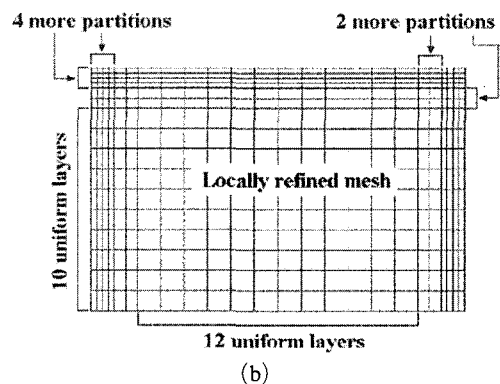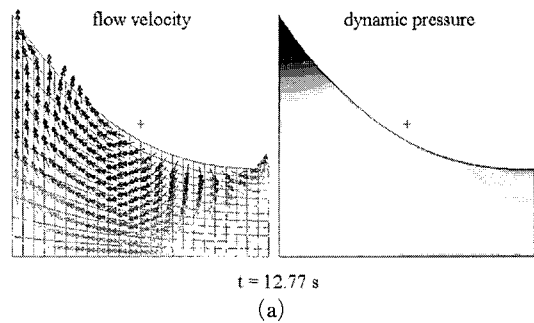
(a)

(b)

Fig. 7 Singularity and mesh refinement : (a) Flow velocity and dynamic pressure fileds (case 1); (b) Local refinement of fluid meshes
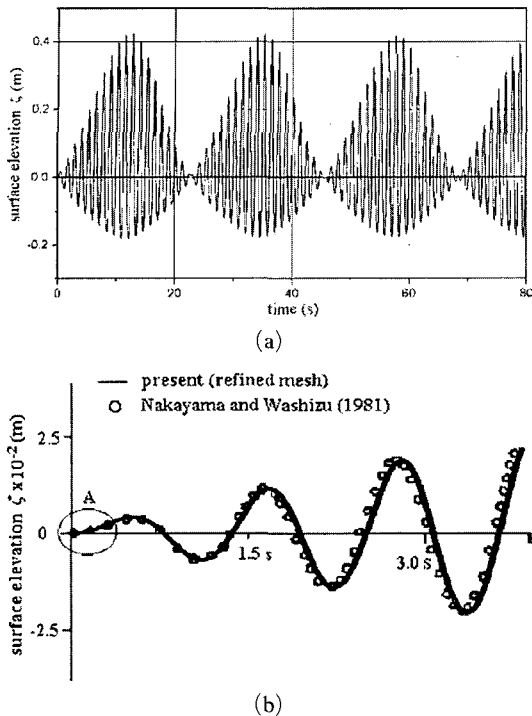
(a)

(b)

Fig. 8 Use of locally refined mesh : (a) Long–time history of the beating phenomenon (case 1); (b) Numerical instability at the beginning (case 2)

amplitudes. As well, the locally refined mesh overcomes the numerical instability occurred at the beginning of the free surface time history response, as represented in Fig. 8(b), where the previous inconsistent downward fluctuation disappears completely.

6. Conclusion

The numerical dissipation and stability of the free surface tracking method devised for the real–time nonlinear finite element analysis of large amplitude sloshing flow have been addressed. The effects of the parameter α introduced for the time differentiation of the free surface elevation and the fluid mesh pattern were intensively examined. Through the numerical experiments we found that the choice of α near 0.1 is most suitable to minimize both the numerical dissipation and the total fluid volume change with time. On the other hand, uniform mesh failed the reliable

simulation of the long–time beating phenomenon and the stable prediction of the initial sloshing time history response. The main reason has been found that uniform mesh can not sufficiently capture the singularity in the flow velocity field. However, the use of locally refined mesh successfully overcome the numerical dissipation in the long–time beating simulation and the numerical instability occurred at the beginning of the sloshing time history response.

Acknowledgments

References

Chen, W., Haroun, M. A. and Liu, F., 1996, "Large Amplitude Liquid Sloshing in Seismically Excited Tanks," *Earthq. Engrg. Struct. Dyn.*, Vol. 25, pp. 653~669.

Cho, J. R. and Lee, S. Y., 2003, "Dynamic Analysis of Baffled Fuel-Storage Tanks Using the ALE Finite Element Method," *Int. J. Numer. Methods Fluids*, Vol. 41, pp. 185~208.

Cho, J. R. and Oden, J. T., 1997, "Locking and Boundary Layer in Hierarchical Models for Thin Elastic Structures," *Comput. Methods Appl. Mech. Engrg.*, Vol. 147, pp. 33~48.

Currie, I. G., 1974, *Fundamental Mechanics of Fluids*, McGraw-Hill, New York.

Faltinsen, O. M., Rognebakke, O. F. and Lukovsky, I. A., 2000, "Multidimensional Modal Analysis of Nonlinear Sloshing in a Rectangular Tank with Finite Water Depth," *J. Fluid Mech.*, Vol. 407, pp. 201~234.

Golub, G. H. and Ortega, J. M., 1992, *Scientific Computing and Differential Equations*, Academic Press, New York.

Kanok-Nukulchai, W. and Tam, B. T., 1999, "Fluid-Structure Interaction Model of Tuned Liquid Damper," *Int. J. Numer. Methods Engng.*, Vol. 46, pp. 1541~1558.

Nakayama, T. and Washizu, K., 1981, "The Boundary Element Method Applied to the Analy-

sis of Two-Dimensional Nonlinear Sloshing Problems," *Int. J. Numer. Methods Engng.*, Vol. 17, pp. 1631~1646.

Okamoto. T. and Kawahara. M.. 1990. "Two-Dimensional Sloshing Analysis by Lagrangian Finite Element Method," *Int. J. Numer. Methods Engng.*, Vol. 11, pp. 453~477.